HHS Public Access

Author manuscript

Langmuir. Author manuscript; available in PMC 2018 December 07.

Published in final edited form as:

Langmuir. 2017 October 10; 33(40): 10525–10530. doi:10.1021/acs.langmuir.7b01362.

Synthesis of Stable Citrate-Capped Silver Nanoprisms

Jason Haber[†,‡] and **Konstantin Sokolov**[*,†,‡,§]

[†]Department of Imaging Physics, UT MD Anderson Cancer Center, 1515 Holcombe Blvd, Houston, Texas 77030, United States

[‡]Department of Biomedical Engineering, University of Texas at Austin, Austin, Texas 78712, United States

[§]Department of Bioengineering, Rice University, 6500 Main Street, Houston, Texas 77030, United States

Abstract

Citrate-stabilized silver nanoprisms (AgNPrs) can be easily functionalized using well-developed thiol based surface chemistry that is an important requirement for biosensor applications utilizing localized surface plasmon resonance (LSPR) and surface-enhanced Raman Scattering (SERS). Unfortunately, currently available protocols for synthesis of citrate-coated AgNPrs do not produce stable nanoparticles thus limiting their usefulness in biosensing applications. Here we address this problem by carrying out a systematic study of citrate-stabilized, peroxide-based synthesis of AgNPrs to optimize reaction conditions for production of stable and reproducible nanoprisms. Our analysis showed that concentration of secondary reducing agent, L-ascorbic acid, is critical to AgNPr stability. Furthermore, we demonstrated that optimization of other synthesis conditions such as stabilizer concentration, rate of silver nitrate addition, and seed dilution result in highly stable nanoprisms with narrow absorbance peaks ranging from 450 nm into near-IR. In addition, the optimized reaction conditions can be used to produce AgNPrs in a one-pot synthesis instead of a previously described two-step reaction. The resulting nanoprisms can readily interact with thiols for easy surface functionalization. These studies provide an optimized set of parameters for precise control of citrate stabilized AgNPr synthesis for biomedical applications.

Graphical Abstract:

[*]**Corresponding Author**, ksokolov@mdanderson.org.

Supporting Information

The Supporting Information is available free of charge on the ACS Publications website at DOI: 10.1021/acs.langmuir.7b01362. Instability calculation; peak-fwhm polynomial regression; representative un-normalized spectra of nanoprisms; effect of hydrogen peroxide on nanoprism spectra and stability; effect of sodium borohydride on absorbance spectra and stability of nanoprisms; nanoprism size analysis based on TEM results; demonstration of one-pot synthesis of silver nanoprisms; comparative absorbance spectra of nanoprisms (PDF)

Notes

The authors declare no competing financial interest.

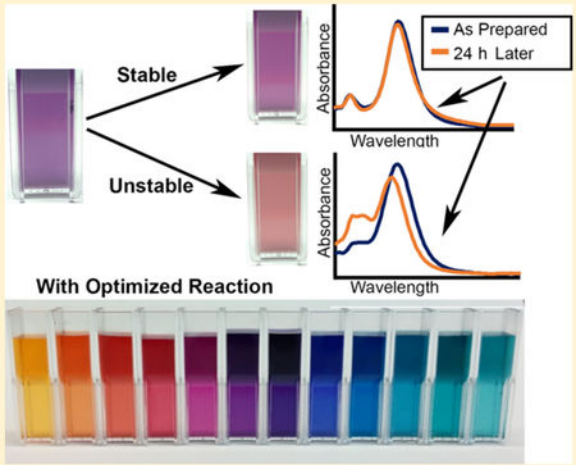

INTRODUCTION

Noble metal nanoparticles with strong plasmon resonance absorbance peaks in the UV-vis-NIR region of the electromagnetic spectrum are highly advantageous in label-free sensor applications, such as those based on localized surface plasmon resonance (LSPR)[1,2] or surface-enhanced Raman scattering (SERS).[3,4] Anisotropy in silver nanoprisms, due to high surface area-to-thickness ratio and sharp edges, results in a resonance peak that shifts strongly with prism size and local dielectric constant,[5,6] which is ideal for such applications. Furthermore, silver nanoprisms synthesis with tunable resonance peaks is important for development of biosensors for multiplex analysis.[7]

Many techniques have been reported for synthesizing silver nanoprisms. In LSPR applications, lithographic techniques are common due to high consistency and ability to functionalize resulting nanostructures,[8,9] but these methods cannot be used in solution-based applications and are not as widely accessible. Solution-based techniques for prism synthesis include photo-induced,[10–12] solvothermal, and seeded growth reduction approaches.[13,14] Many chemical methods rely on reducing agents, such as sodium borohydride, in conjunction with some form of capping agent such as bis(*p*-sulfonatophenyl)-phenylphosphine (BSPP), polyvinylpirrolidine (PVP),[15–17] or dextran.[18] Although these approaches result in stable nanoprisms, the strength of capping agent binding leads to difficulty in functionalization of resulting nanoparticles for sensor applications.[19,20] To address this problem, other methods were developed that use etchants such as hydrogen peroxide in combination with a weakly bound capping agent[21,22] to allow easy surface functionalization using ligand exchange. However, without a strong capping agent, these protocols produce nanoprisms with inadequate reproducibility and lack of stability severely limiting their utility in bioapplications. Therefore, despite a significant body of work in synthesis of plasmonic nanoprisms, there is still need to develop a robust protocol to produce stable and reproducible nanoprisms that are amenable for an easy surface functionalization.

Here we report a systemic investigation of citrate-stabilized, hydrogen peroxide based synthesis of silver nanoprisms to determine the effects of all reagents on stability and

reproducibility of resulting nanoparticles. Our results showed that concentration of secondary reducing agent, L-ascorbic acid, is the most important parameter in controlling stability of silver nanoprisms (AgNPrs). Furthermore, we demonstrated that synthesis of stable citrate-capped AgNPrs is possible and determined optimum reaction conditions for making tunable and stable nanoprisms with plasmon resonance ranging from 450 to 900 nm.

EXPERIMENTAL SECTION

Chemicals.

From Sigma-Aldrich: Silver nitrate (99.9999% trace metals basis), sodium citrate dihydrate, L-ascorbic acid, hydrogen peroxide (30%), sodium borohydride, 2-propanol, (3-mercaptopropyl)trimethoxysilane, poly-L-lysine (0.1% aqueous solution).

Optimized Synthesis of Stable Silver Nanoplates (Aged Seeds).

Prior to synthesis, all reagent solutions were prepared fresh. In a typical experiment, a solution consisting of 39.3 mL of diH_2O, 2 mL of trisodium citrate (TSC) (75 mM), 256 μL of hydrogen peroxide (H_2O_2) (0.6%), and 186 μL of silver nitrate ($AgNO_3$) (10 mM) was prepared. Under vigorous stirring, 192 μL of sodium borohydride ($NaBH_4$) (100 mM) was rapidly added to initiate reduction, and the solution immediately changed to a pale yellow color. After 5 min, the color shifted to a golden yellow. Then, the solution was stored overnight at room temperature. Following this aging period, 2.1 mL of the seed stock was added to a clean 8 mL vial and stirred vigorously. Then 200 μL of L-ascorbic acid (5 mM) was added to this mixture, followed by addition of $AgNO_3$ (10 mM) dropwise until the desired solution color was reached (typically 100 μL).

Flow Rate Experiments.

The same protocol as above was followed to prepare the nanoparticle seeds. For nanoprism formation, 2.1 mL of the seed stock were added to a clean 8 mL vial and stirred vigorously. Then 200 μL of L-ascorbic acid (5 mM) was added to this mixture. A KD Scientific syringe pump was then used to inject 100 μL of $AgNO_3$ at a controlled rate ranging from 15 to 400 μL/min.

Synthesis of Larger Nanoplates.

Larger nanoplates were synthesized by diluting seed solution prior to addition of L-ascorbic acid and silver nitrate. Seed solutions were prepared proportionally in smaller quantities and then diluted by addition of diH_2O to reach 2.1 mL. The reaction then proceeded as above. Typically, dilutions were used as follows: 1× for nanoplates with absorbance peaks up to ~550 nm, 1/2× for ~550–590 nm (1.05 mL of seed stock, 1.05 mL of diH_2O), 1/4× for ~590–630 nm, 1/8× for ~630–700 nm, and 1/12× for NIR nanoplates.

Characterization.

Characterization of the size and morphology of silver prisms was performed using transmission electron microscopy (TEM). Samples were placed as drops onto 100 mesh Formvar/carbon coated copper for approximately 1 h. Samples were blotted dry from the

grids with filter paper and were allowed to dry. Samples were then examined in a JEM 1010 transmission electron microscope (JEOL, USA, Inc., Peabody, MA) at an accelerating voltage of 80 KV. Digital images were obtained using the AMT Imaging System (Advanced Microscopy Techniques Corp., Danvers, MA). Optical spectra were acquired using a BioTek SynergyHT UV–vis spectrometer. Absorbance spectra were normalized to have an area-under-the-curve (AUC) of 1.

Nanoprism Stability.

Changes in absorbance spectra of nanoparticle samples were used as an indicator of stability in solution. The changes were quantified by first normalizing both initial absorbance spectrum of a nanoplate solution and the one obtained after 24 h by their AUC to obtain area-weighted spectra. Relative spectral changes were then calculated as the disagreement between the two spectra expressed as a percentage of the agreement according to the formula instability = $I_{\text{init}} \oplus I_{24\text{h}}/I_{\text{init}} \cap I_{24\text{h}}$, i.e., the difference between the two spectra expressed as a ratio of their area of overlap. This formula is a variant of the Jaccard Index[23] intended to highlight dissimilarity between two spectral curves (see the Supporting Information for derivation). Disagreement between two spectra can be expressed as the absolute value of their differences, or $I_{\text{init}} \oplus I_{24\text{h}} = \sum|I^n_{\text{init}} - I^n_{24\text{h}}|$ where I^n_{init} and $I^n_{24\text{h}}$ are optical densities at nth wavelength of the initial spectrum and the spectrum taken at 24 h, respectively, and the sum is over the whole wavelength region. The agreement can be expressed as the sum of the two spectra minus their disagreement, or $I_{\text{init}} \cap I_{24\text{h}} = \sum I^n_{\text{init}} + I^n_{24\text{h}} - \sum|I^n_{\text{init}} - I^n_{24\text{h}}|$. For spectra normalized to an AUC of 1, this becomes $I_{\text{init}} \cap I_{24\text{h}} = 2 - \sum|I^n_{\text{init}} - I^n_{24\text{h}}|$. Therefore, nanoprism instability was calculated using the equation instability = $\left(\sum|I^n_{\text{init}} - I^n_{24\text{h}}|\right) \Big/ \left(2 - \sum|I^n_{\text{init}} - I^n_{24\text{h}}|\right)$. Ideal stability (i.e., no change in the absorbance spectrum) would result in instability = 0 according to this calculation. Anything below 0.08 was considered to be stable due to only minor observable changes in the spectra.

Nanoprism Adhesion to Glass Substrates.

A solution of 2% w/w (3-mercaptopropyl)trimethoxysilane (MPTMS), 5% diH_2O in 2-propanol was prepared. Standard glass microscope slides were treated with 0.05 M sodium hydroxide for 30 min at 80 °C and then washed with diH_2O. The MPTMS solution was evenly distributed on the surface of the slides and placed in a sealed Petri dish in an oven heated to 90 °C for 2 h, which vaporized the MPTMS solution and allowed for an even surface coating. The slides were then removed from the oven and washed in diH_2O before being left in the nanoprism solution overnight. After the overnight incubation, the slides with nanoprism monolayers were removed and washed in diH_2O. The slides with AgNPr monolayers can be stored in diH_2O solution to prevent drying.

Optimized One-Pot Synthesis.

A solution was prepared consisting of 1.965 mL of diH_2O, 100 μL of TSC (75 mM), 9.3 μL of $AgNO_3$ (10 mM), and 12.8 μL of H_2O_2 (0.6%). Under vigorous stirring, 9.6 μL of $NaBH_4$ (100 mM) was added rapidly. After about 5 min, the color shifted to a golden yellow. Then,

200 μL of L-ascorbic acid (5 mM) was added, followed by dropwise addition of $AgNO_3$ (10 mM) until the desired nanoplate size had been reached (typically 50–150 μL).

RESULTS AND DISCUSSION

In a typical two-step peroxide-etchant synthesis, seed stock is, first, prepared using silver nitrate ($AgNO_3$), hydrogen peroxide (H_2O_2), trisodium citrate (TSC), and sodium borohydride ($NaBH_4$), a reducing agent. The seeds are aged overnight and diluted in diH_2O, and then L-ascorbic acid is added prior to prism growth with dropwise addition of $AgNO_3$. The problem is that this reaction results in silver nanoprisms that degrade within 24 h; this is associated with large changes in their absorbance spectra including an increase in the 400 nm peak indicative of small silver nanospheres as shown in Figure 1. Note that there is no significant change in the absolute peak intensity over time, indicating that instability is associated mostly with morphological changes of the nanoparticles (Supporting Information Figure S1).

To determine whether H_2O_2-mediated seeded-growth method can be optimized to achieve synthesis of stable citrate-capped nanoprisms in a broad range of sizes and corresponding plasmon resonance peaks, we assayed all reagents and reaction conditions in the synthesis that is schematically shown in Figure 2.

First, L-ascorbic acid was evaluated, the prism growth stage reducing agent. It has been reported that hydrogen peroxide prevents $NaBH_4$ from interfering with prism growth, eliminating the need for overnight aging.[19] Therefore, we evaluated synthesis with fresh (Figure 3a and c) and aged-overnight seed (Figure 3b and d) solutions. As shown in Figure 3a and b, ascorbic acid concentration above ~0.1 mM was required for prism growth, and little spectral change was observed above this concentration. However, after 24 h, samples with high ascorbic acid concentration (>6 mM) showed significant change in spectrum shape that was more pronounced for fresh seeds (Figure 3c), indicating lack of stability. This spectral change was quantified as instability = $I_{init} \oplus I_{24h}/I_{init} \cap I_{24h}$ where disagreement ($\oplus$) between initial (I_{init}) and 24 h (I_{24h}) spectra was divided by agreement ($\cap$); i.e., the difference between the two spectra expressed as a ratio of their area of overlap (see more details in the Supporting Information). This characteristic serves as a measure of similarity between two curves that accounts for both shifts in relative peak intensity and peak location, and was used as an indicator of stability throughout this study. Scores below 0.08 were considered stable, as they correlated with very small spectral changes (examples in Figure 3c and d, blue spectra). Ascorbic acid concentrations from 0.435 to 1.74 mM resulted in the most stable nanoprisms, with the optimum concentration at 0.435 mM. Stability at high ascorbic acid concentrations was significantly better in samples prepared using aged seeds, though this effect was negligible with reduced ascorbic acid concentration (Figure 3e). These results show that excess of ascorbic acid greatly decreases stability of nanoprisms. This effect is likely due to the role of ascorbic acid as a reducing agent; higher concentrations have been hypothesized to favor formation of alternative nanoparticle shapes.[24] Further experiments were performed using aged seeds due to better stability across the range of ascorbic acid concentrations.

Next, we studied the effects of hydrogen peroxide, an etchant, and sodium borohydride, the reducing agent for initial seed production, on prism synthesis and stability. Nanoprisms with the smallest secondary peak at 400 nm resulted from seed preparations made using the range of H_2O_2 concentrations from 88 to 121 μM (Figure S2). $NaBH_4$ concentrations above ~250 μM were required for ideal nanoprism growth (Figure S3). Varying of neither H_2O_2 nor $NaBH_4$ concentrations impacted nanoprism stability (Figures S2 and S3). While sodium borohydride is a reducing agent, it decomposes rather quickly in an aqueous solution and, therefore, does not influence long-term stability of nanoprisms.[19] Hydrogen peroxide is an etchant that promotes growth of planar twinned seeds which favor the anisotropic growth necessary for nanoprism formation.[18] It is believed to mostly impact the ability of the synthesis to form prism structures rather than long-term stability.

It was observed that, during prism growth, addition of silver nitrate beyond 1/10 of initial reaction volume resulted in no further growth, preventing synthesis of larger prisms. To address this, the effect of seed concentration was evaluated in the context of increasing nanoprism size. As shown in Figure 4a, diluting seed stock resulted in larger nanoprisms with absorbance peaks up to 900 nm. Continuous growth of larger nanoparticles indicate that the reaction is maintained under the diffusion-controlled condition, with silver ion concentration below the supersaturation point.[25] The data also show that decreasing the seed concentration allows for a larger quantity of silver ions to be incorporated into each particle under these reaction conditions (Figure 4c). Further increase in silver ion concentration could lead to supersaturation, which is associated with secondary nucleation rather than the diffusion-controlled growth of nanoprisms.[25] Optimal stability of large nanoprisms was observed at 0.435 mM ascorbic acid concentration (Figure 4b), indicating that ideal concentration of ascorbic acid was invariant with seed concentration.

Next, we analyzed the effects of trisodium citrate (TSC), a capping agent (Figure 5). For small prism sizes (<35 nm edge length, see Figure S4), varying TSC concentration resulted in little difference in spectra (Figure 5a). For larger prisms, peaks broadened significantly at lower TSC concentrations (Figure 5b). Sodium citrate acts as a surface stabilizer, binding to facets and preventing addition of silver ions, thus halting nanoprism growth.[26,27] Therefore, we hypothesized that higher concentrations of sodium citrate were required for synthesis of larger nanoprisms with more consistent morphology.

To verify this assumption, nanoprisms were synthesized with TSC concentrations ranging from 0.71 to 5.36 mM. For each concentration, nanoprisms were grown with absorbance peaks ranging from 450 to 780 nm by changing the quantity of silver nitrate added. Then peak full-width at half-maximum (peak-fwhm) was used as an indicator of dispersity (Figure 5c). This metric, peak-fwhm, has been previously evaluated and applied to characterization of dispersity of silver nanoparticles.[25] The narrowest peak-fwhm (~80 nm) occurred for small nanoprisms (~30 nm edge length) at all TSC concentrations. As expected, peak-fwhm increased faster with prism size for lower TSC concentrations, indicating more variation in particle morphologies under these conditions.

Finally, rate of silver nitrate addition during prism growth was analyzed. Silver nitrate was added to the seed solution by an automated syringe pump at flow rates from 15 to 400 μL/

min. Three formulations were used: (i) 3.57 mM TSC (base reaction condition, Figure 1), (ii) 0.71 mM TSC (reduced citrate), and (iii) 1/2 seed stock concentration (as in Figure 2, but, diluted seeds for larger nanoprisms). Slower rate of addition was better under all conditions; this was evident from a reduced secondary peak at 400 nm and red-shifted spectra indicating increased silver incorporation (Figure 6). Higher rates of silver nitrate addition likely exceed the rate of silver incorporation into nanoprisms that has a negative correlation with the concentration of the capping agent (TSC), leading to an increase of the absorbance peak at 400 nm indicative of formation of silver nanospheres. Indeed, significantly slower rates of silver nitrate addition of ca. 50 μL/min are required at higher TSC concentration of 3.57 mM (Figure 6a) to diminish the 400 nm peak as compared to less than 200 μL/min at lower TSC concentration of 0.71 mM (Figure 6c). Little improvement in nanoprism quality was observed below a rate of ca. 50 μL/min in all conditions. Flow rate had very little effect on nanoprism stability, as instability values were consistently around or below 0.08. (Figure 6d).

Using optimized parameters from our experiments, we developed a protocol for synthesis of stable silver nanoprisms in a wide range of sizes (Figure 7) exhibiting plasmon resonance peaks covering the visible and near-infrared (NIR) spectral region (Figure 8a and b). To verify that nanoprisms prepared with this protocol can be used for surface functionalization using thiol chemistry, the nanoparticles were adhered to a glass slide coated with (3-mercaptopropyl) trimethoxysilane (MPTMS). Nanoprisms formed a uniform dense layer on the MPTMS-coated glass slide through interactions with thiol groups (Figure 8b). No nanoprisms adhered to control slides that were not coated with MPTMS.

Since nanoprisms synthesized from fresh seeds were stable at low ascorbic acid concentrations, we demonstrated a one-pot variant of the optimized protocol described here for stable nanoprism synthesis (Figure S5), in which seed solution is used for prism growth without the aging step. The protocol produced stable nanoprisms, and it was fully scalable in synthesis volumes ranging from 2.3 to 46 mL prior to silver nitrate addition (Figure S6).

CONCLUSIONS

In summary, we systematically tested seed-mediated synthesis of citrate-stabilized silver nanoprisms to determine the feasibility of production of stable citrate-capped nanoparticles for easy surface functionalization. We demonstrated greatly increased nanoparticle stability by controlling ascorbic acid concentration. Aging of the seed solution was also important at higher concentrations of ascorbic acid as can be seen in Figure 3e most likely due to incomplete decomposition of sodium borohydride in freshly prepared seed solutions. These results indicate that an excess of reducing agents is a major contributor to instability in nanoprism suspensions.

In addition, tight control of nanoprism synthesis was achieved through optimization of seed dilution, citrate concentration, and rate of silver nitrate addition. Using optimized parameters, we developed a scalable, refined protocol for silver nanoprisms with fully tunable plasmon resonances across the visual and near-infrared wavelength range. We demonstrated that these particles can be used for surface functionalization in future

biosensor applications using thiol chemistry. Furthermore, we validated extension of the developed protocol to a one-pot synthesis of stable nanoprisms.

Supplementary Material

Refer to Web version on PubMed Central for supplementary material.

ACKNOWLEDGMENTS

This work supported in part by NIH Grant R01 CA103830. TEM characterization by the High Resolution Microscopy Facility (HREMF) at MD Anderson, supported by CCSG Grant NIH P30CA016672.

REFERENCES

(1). Anker JN; Hall WP; Lyandres O; Shah NC; Zhao J; Van Duyne RP Biosensing with plasmonic nanosensors. Nat. Mater 2008, 7 (6), 442–453. [PubMed: 18497851]

(2). Forestiere C; Pasquale AJ; Capretti A; Miano G; Tamburrino A; Lee SY; Reinhard BRM; Dal Negro L Genetically engineered plasmonic nanoarrays. Nano Lett. 2012, 12 (4), 2037–2044. [PubMed: 22381056]

(3). Ciou SH; Cao YW; Huang HC; Su DY; Huang CL SERS enhancement factors studies of silver nanoprism and spherical nanoparticle colloids in the presence of bromide ions. J. Phys. Chem. C 2009, 113 (22), 9520–9525.

(4). Farhadi A; Roxin A; Wilson BC; Zheng G Nano-enabled SERS reporting photosensitizers. Theranostics 2015, 5 (5), 469. [PubMed: 25767614]

(5). Kelly KL; Coronado E; Zhao LL; Schatz GC The optical properties of metal nanoparticles: the influence of size, shape, and dielectric environment. J. Phys. Chem. B 2003, 107 (3), 668–677.

(6). Eustis S; El-Sayed MA Why gold nanoparticles are more precious than pretty gold: noble metal surface plasmon resonance and its enhancement of the radiative and nonradiative properties of nanocrystals of different shapes. Chem. Soc. Rev 2006, 35 (3), 209–217. [PubMed: 16505915]

(7). Gao S; Koshizaki N; Tokuhisa H; Koyama E; Sasaki T; Kim JK; Ryu J; Kim DS; Shimizu Y Highly stable Au nanoparticles with tunable spacing and their potential application in surface plasmon resonance biosensors. Adv. Funct. Mater 2010, 20 (1), 78–86.

(8). Haes AJ; Haynes CL; McFarland AD; Schatz GC; Van Duyne RP; Zou S Plasmonic materials for surface-enhanced sensing and spectroscopy. MRS Bull. 2005, 30 (05), 368–375.

(9). Shin DO; Jeong JR; Han TH; Koo CM; Park HJ Lim YT Kim SO A plasmonic biosensor array by block copolymer lithography. J. Mater. Chem 2010, 20 (34), 7241–7247.

(10). Jin R; Cao YC; Hao E; Métraux GS; Schatz GC; Mirkin CA Controlling anisotropic nanoparticle growth through plasmon excitation. Nature 2003, 425 (6957), 487–490. [PubMed: 14523440]

(11). Bastys V; Pastoriza-Santos I; Rodríguez-González B; Vaisnoras R; Liz-Marzán LM Formation of silver nanoprisms with surface plasmons at communication wavelengths. Adv. Funct. Mater 2006, 16 (6), 766–773.

(12). Xue C; Métraux GS; Millstone JE; Mirkin CA Mechanistic study of photomediated triangular silver nanoprism growth. J. Am. Chem. Soc 2008, 130 (26), 8337–8344. [PubMed: 18533653]

(13). Aherne D; Ledwith DM; Gara M; Kelly JM Optical properties and growth aspects of silver nanoprisms produced by a highly reproducible and rapid synthesis at room temperature. Adv. Funct. Mater 2008, 18 (14), 2005–2016.

(14). Yang Y; Matsubara S; Xiong L; Hayakawa T; Nogami M Solvothermal synthesis of multiple shapes of silver nanoparticles and their SERS properties. J. Phys. Chem. C 2007, 111 (26), 9095–9104.

(15). Métraux GS; Mirkin CA Rapid thermal synthesis of silver nanoprisms with chemically tailorable thickness. Adv. Mater 2005, 17 (4), 412–415.

(16). Tsuji M; Gomi S; Maeda Y; Matsunaga M; Hikino S; Uto K; Tsuji T; Kawazumi H Rapid transformation from spherical nanoparticles, nanorods, cubes, or bipyramids to triangular prisms

of silver with PVP, citrate, and H2O2. Langmuir 2012, 28 (24), 8845–8861. [PubMed: 22506506]

(17). Zhang Q; Hu Y; Guo S; Goebl J; Yin Y Seeded growth of uniform Ag nanoplates with high aspect ratio and widely tunable surface plasmon bands. Nano Lett. 2010, 10 (12), 5037–5042. [PubMed: 21038884]

(18). Parnklang T; Lertvachirapaiboon C; Pienpinijtham P; Wongravee K; Thammacharoen C; Ekgasit S H2O2-triggered shape transformation of silver nanospheres to nanoprisms with controllable longitudinal LSPR wavelengths. RSC Adv. 2013, 3 (31), 12886–12894.

(19). Li N; Zhang Q; Quinlivan S; Goebl J; Gan Y; Yin Y H2O2-Aided Seed-Mediated Synthesis of Silver Nanoplates with Improved Yield and Efficiency. ChemPhysChem 2012, 13 (10), 2526–2530. [PubMed: 22298378]

(20). Sherry L; Jin R; Mirkin C; Schatz G; Van Duyne RP Localized surface plasmon resonance spectroscopy of single silver triangular nanoprisms. Nano Lett. 2006, 6, 2060–2065. [PubMed: 16968025]

(21). Zhang Q; Li N; Goebl J; Lu Z; Yin Y A systematic study of the synthesis of silver nanoplates: is citrate a “magic” reagent? J. Am. Chem. Soc 2011, 133 (46), 18931–18939. [PubMed: 21999679]

(22). Torres V; Popa M; Crespo D; Moreno JMC Silver nanoprism coatings on optical glass substrates. Microelectron. Eng 2007, 84 (5), 1665–1668.

(23). Varmuza K; Karlovits M; Demuth W Spectral similarity versus structural similarity: infrared spectroscopy. Anal. Chim. Acta 2003, 490 (1), 313–324.

(24). Sau TK; Murphy CJ Room temperature, high-yield synthesis of multiple shapes of gold nanoparticles in aqueous solution. J. Am. Chem. Soc 2004, 126 (28), 8648–8649. [PubMed: 15250706]

(25). Zong R; Wang X; Shi S; Zhu Y Kinetically controlled seed-mediated growth of narrow dispersed silver nanoparticles up to 120 nm: secondary nucleation, size focusing and Ostwald ripening. Phys. Chem. Chem. Phys 2014, 16, 4236–4241. [PubMed: 24452515]

(26). Li H; Xia H; Wang D; Tao X Simple synthesis of monodisperse, quasi-spherical, citrate-stabilized silver nanocrystals in water. Langmuir 2013, 29 (16), 5074–5079. [PubMed: 23578217]

(27). Zeng J; Zheng Y; Rycenga M; Tao J; Li Z-Y; Zhang Q; Zhu Y; Xia Y Controlling the shapes of silver nanocrystals with different capping agents. J. Am. Chem. Soc 2010, 132, 8552–8553. [PubMed: 20527784]

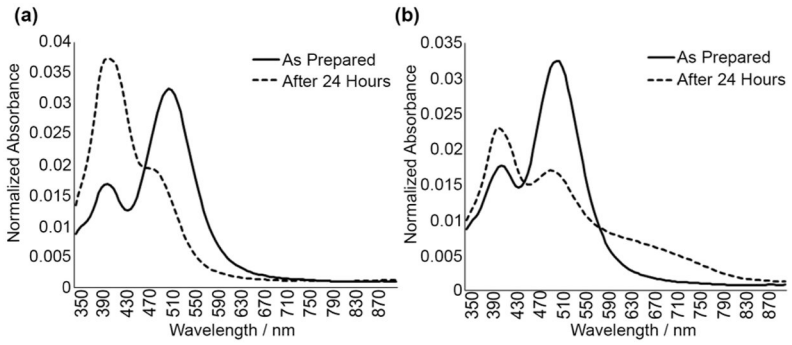

Figure 1.

Representative examples of absorbance spectra of citrate-capped silver nanoprisms synthesized using common peroxide-etchant method: as prepared (solid line) and after 24 h (dashed line). Significant changes in absorbance spectra over time indicate a lack of stability. Panels (a) and (b) illustrate two different ways in which nanoprisms can degrade: (a) degradation to silver nanospheres and (b) degradation to nanosphers with aggregation that is evident by an increase absorbance in the red-NIR spectral region.

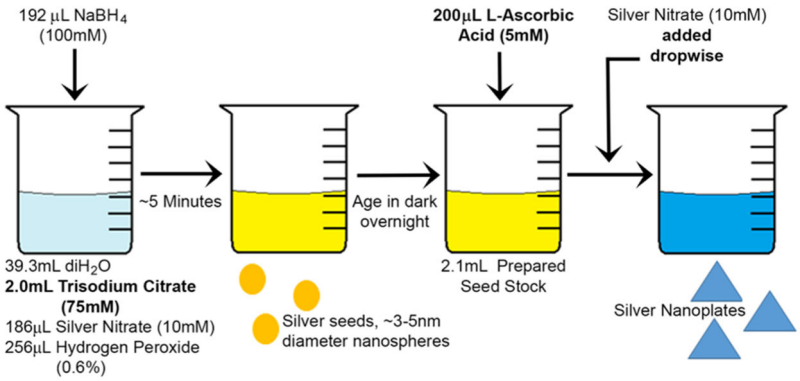

Figure 2.

Reaction schematic of optimized citrate-stabilized nanoprism synthesis using peroxide etching. All listed reaction components were evaluated here, and those found to have significant effect on stability and reproducibility of silver nanoprisms are highlighted in bold.

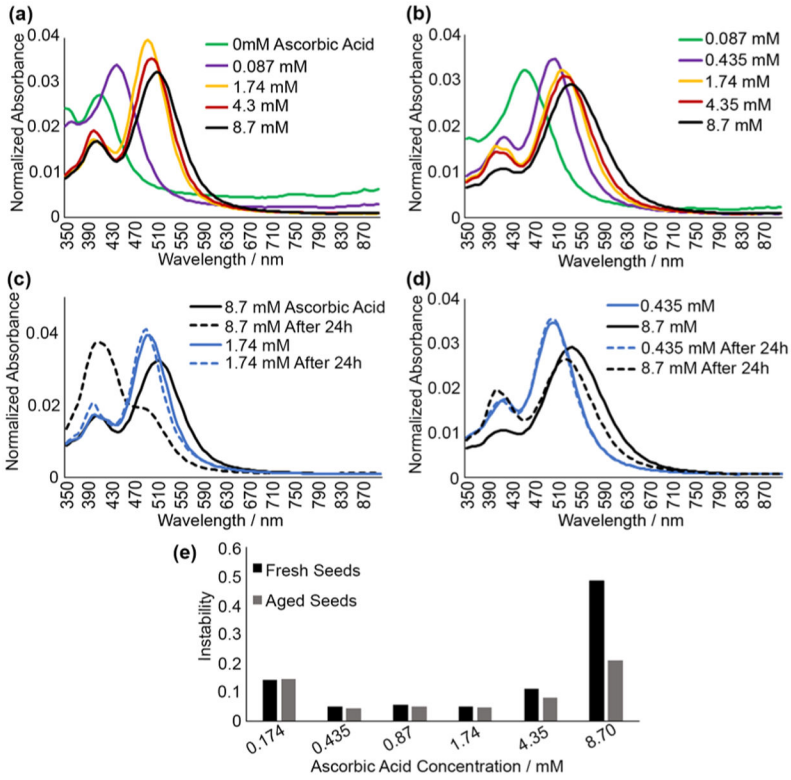

Figure 3.

Spectra (normalized to AUC of 1) demonstrating effects of varying ascorbic acid in nanoprism synthesis with fresh (a) and aged (b) seed solutions. Representative examples of stable (1.74 mM ascorbic acid, blue) and unstable (8.7 mM ascorbic acid, black) nanoprisms prepared using fresh (c) and aged (d) seeds; note spectral changes 24 h after synthesis in samples with 8.7 mM ascorbic acid. 24 h stability test for nanoprisms prepared using various concentrations of ascorbic acid with either aged or fresh seeds (e); note high nanoprism stability for ascorbic acid concentrations ranging from 0.435 to 1.74 mM.

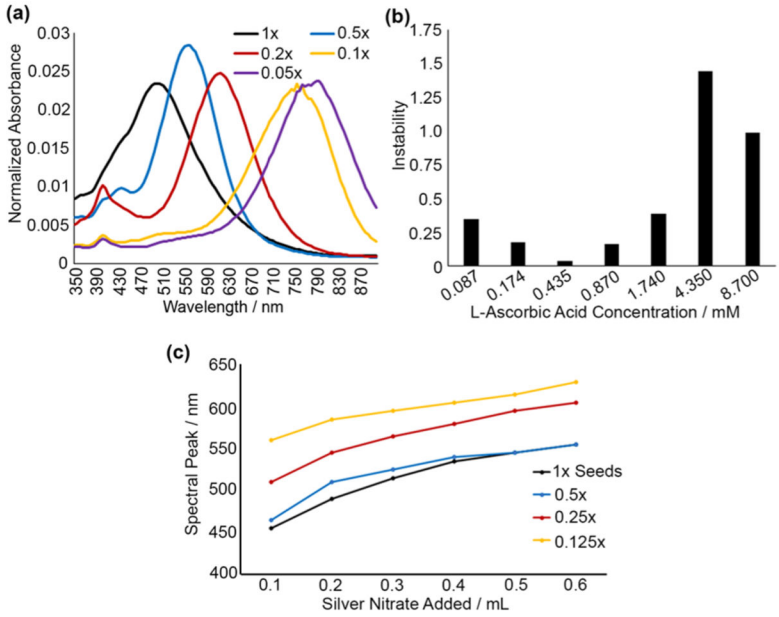

Figure 4.

(a) Absorbance spectra demonstrating effects of seed dilution on nanoprism growth with seed concentrations 1×, 0.5×, 0.2×, 0.1×, and 0.05× of initially prepared seed stock. All experiments were performed with dropwise addition of 100 μL of silver nitrate. (b) 24 h stability test for nanoprisms prepared from 0.1× seed solution with varying ascorbic acid concentration. (c) Absorbance peak of silver nanoprisms as a function of volume of silver nitrate added for different dilutions (1×, 0.5×, 0.25×, and 0.125×) of seed stock. All data points correspond to 10.5 mL initial solution. Note that increased levels of dilution allow for growth of larger nanoprisms while using the same quantity of silver nitrate.

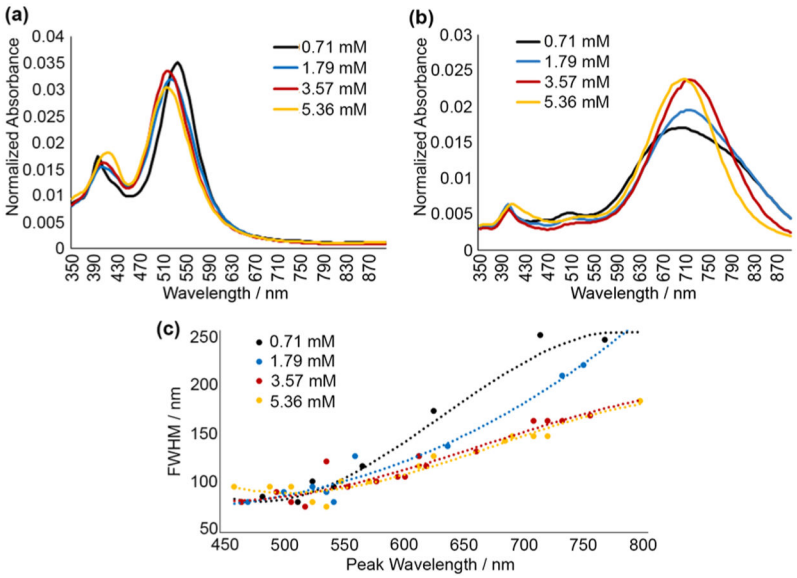

Figure 5.

(a) Absorbance spectra of small nanoprisms (~30 nm edge length) prepared from aged seeds with varied concentration of trisodium citrate (TSC). Reactions proceed faster with lower TSC concentration, but optical properties remain unchanged. (b) Spectra of larger nanoprisms (~100 nm edge length) prepared using varied TSC concentration. Note widening of plasmonic peaks at lower citrate concentrations. (c) Scatter plot of peak full-width at half-maximum (peak-fwhm) as a function of absorbance peak wavelength for varied TSC concentrations; note a relative increase in peak-fwhm for larger nanoprisms at lower TSC concentrations. Dotted lines show polynomial fits for each scatter plot (see the Supporting Information for details).

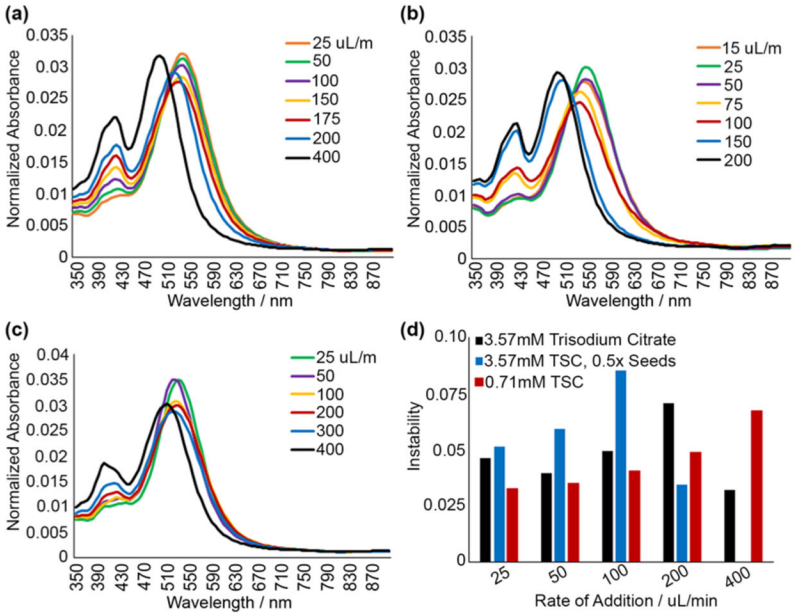

Figure 6.

Absorbance spectra demonstrating effects of varying rate of silver nitrate addition in the case of (a) 3.57 mM TSC seed solution; (b) 3.57 mM TSC with seed solution diluted two-times; and (c) 0.71 mM TSC seed solution. (d) Relative spectral changes after 24 h demonstrating stability of nanoprisms for conditions tested.

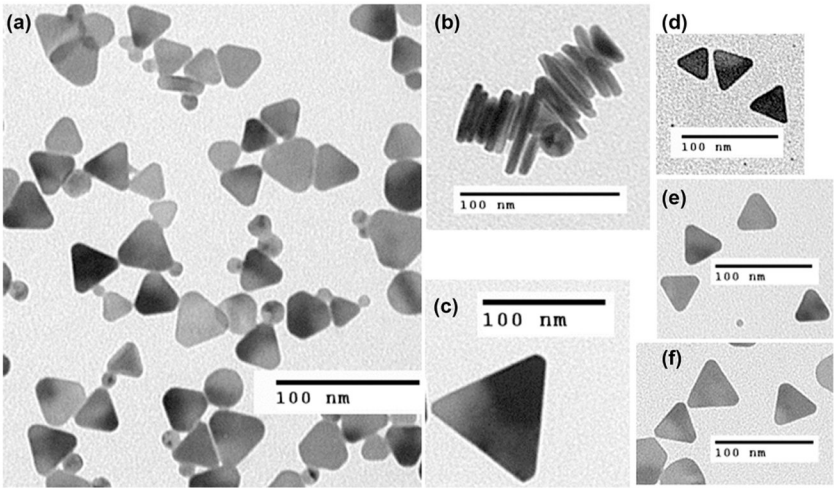

Figure 7.

(a) Representative TEM image of synthesized nanoprisms. (b)TEM showing stacked nanoprisms; plate thickness is ca. 7 nm. (c–f) Representative TEM images showing nanoprisms with sizes 105 nm (c), 40 nm (d), 45 nm (e), and 50 nm (f).

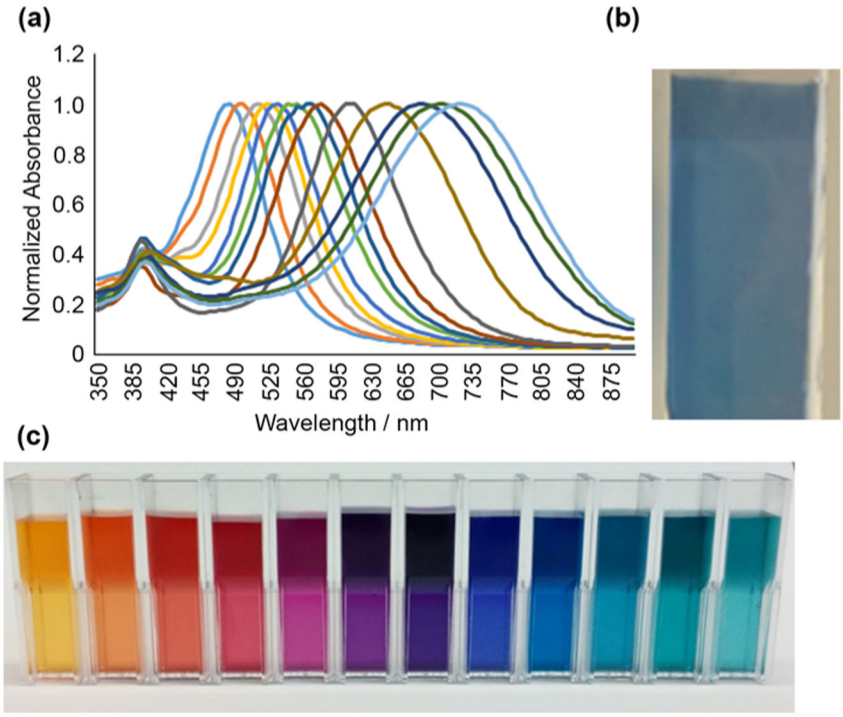

Figure 8.

(a) Absorbance spectra (normalized to peak absorbance of 1) for a subset of nanoprisms synthesized using the optimized citrate-stabilized nanoprism synthesis described here. (b) Thiol-modified glass slide uniformly coated with ~50 nm edge length nanoprisms. (c) Nanoprism suspensions in water demonstrating a range of particle colors.